6-5-2019

Improving the Stability and Monodispersity of Layered Cesium Lead Iodide Perovskite Thin Films by Tuning Crystallization Dynamics

Atefe Hadi
Iowa State University, atefe@iastate.edu

Bradley J. Ryan
Iowa State University, bryan@iastate.edu

Rainie D. Nelson
Iowa State University, rainie@iastate.edu

See next page for additional authors

Improving the Stability and Monodispersity of Layered Cesium Lead Iodide Perovskite Thin Films by Tuning Crystallization Dynamics

Abstract

Assembling halide perovskites into layered structures holds promise for addressing chemical and phase stability challenges; however, several other challenges need to be addressed to create efficient and stable halide perovskite devices. Layered halide perovskites (LHPs) suffer from broad distribution of layer thicknesses and bandgaps within thin films. Reducing polydispersity could substantially improve charge transport within LHP films and the performance of LHP-based solar cells. Herein, we focused on layering α-CsPbI3 ((C4H9NH3)2Csn-1PbnI3n+1) thin films. We found that (C4H9NH3)2Csn-1PbnI3n+1 with nominal layer thicknesses of n = 1, 2, 3, and 4 can be deposited at temperatures as low as 100 °C, substantially below the phase transition temperature of bulk α-CsPbI3. Furthermore, we demonstrated that incorporating highly complexing solvents into the precursor solution promotes the formation of intermediate phases within the thin film, slowing down LHP crystallite nucleation, eventually resulting in improved phase purity. Reducing decomposition rates through combined use of solvent complexes and thermal processing methods, we fabricated (C4H9NH3)2CsPb2I7 films that had improved phase purity, crystallinity, and film morphology. We also demonstrate that the photoluminescence had a maximum intensity corresponding to the targeted n = 2 phase. This work represents a step towards highly stable LHP thin films with narrow site-energy distribution.

Disciplines

Materials Chemistry | Membrane Science | Nanoscience and Nanotechnology

Comments

This document is the unedited Author's version of a Submitted Work that was subsequently accepted for publication in *Chemistry of Materials*, copyright © American Chemical Society after peer review. To access the final edited and published work see DOI: 10.1021/acs.chemmater.9b00238. Posted with permission.

Authors

Atefe Hadi, Bradley J. Ryan, Rainie D. Nelson, Kalyan Santra, Fang-Yi Lin, Eric W. Cochran, and Matthew G. Panthani

Improving the Stability and Monodispersity of Layered Cesium Lead Iodide Perovskite Thin Films by Tuning Crystallization Dynamics

Atefe Hadi,[†] Bradley J. Ryan,[†] Rainie D. Nelson,[†] Kalyan Santra,[‡, §] Fang-Yi Lin,[†] Eric W. Cochran,[†] and Matthew G. Panthani[*,†]

†Department of Chemical and Biological Engineering, Iowa State University, Ames, IA 50011, United States

‡Department of Chemistry, Iowa State University, Ames, IA 50011, United States

[§]U.S. Department of Energy, Ames Laboratory, Ames, IA 50011, United States

ABSTRACT: Assembling halide perovskites into layered structures holds promise for addressing chemical and phase stability challenges; however, several other challenges need to be addressed to create efficient and stable halide perovskite devices. Layered halide perovskites (LHPs) suffer from broad distribution of layer thicknesses and bandgaps within thin films. Reducing polydispersity could substantially improve charge transport within LHP films and the performance of LHP-based solar cells. Herein, we focused on layering α-$CsPbI_3$ ($(C_4H_9NH_3)_2Cs_{n-1}Pb_nI_{3n+1}$) thin films. We found that $(C_4H_9NH_3)_2Cs_{n-1}Pb_nI_{3n+1}$ with nominal layer thicknesses of n = 1, 2, 3, and 4 can be deposited at temperatures as low as 100 °C, substantially below the phase transition temperature of bulk α-$CsPbI_3$. Furthermore, we demonstrated that incorporating highly complexing solvents into the precursor solution promotes the formation of intermediate phases within the thin film, slowing down LHP crystallite nucleation, eventually resulting in improved phase purity. Reducing decomposition rates through combined use of solvent complexes and thermal processing methods, we fabricated $(C_4H_9NH_3)_2CsPb_2I_7$ films that had improved phase purity, crystallinity, and film morphology. We also demonstrate that the photoluminescence had a maximum intensity corresponding to the targeted n = 2 phase. This work represents a step towards highly stable LHP thin films with narrow site-energy distribution.

INTRODUCTION

Lead (Pb) halide perovskites have excellent optoelectronic properties[1-4] and have demonstrated extraordinary laboratory-scale performance in a variety of optoelectronic applications. This high performance combined with their potential for low-cost processing makes Pb-halide perovskites appealing for future electronic and photonic applications.[5-8] Hybrid Pb-halide perovskites, with the chemical formula of ABX_3, have Pb as a divalent B-site cation, halides as the X-site anion, and organic species as the A-site cation. Solar cells fabricated using halide perovskite absorber layers have demonstrated power conversion efficiencies (PCEs) of 24.2%;[9] however, their instability upon exposure to moisture, light, and heat has posed a challenge to commercializing these materials[10-13] and has inspired research focused on improving the stability of halide perovskite devices. One promising route to improving the moisture stability has been the incorporation of hydrophobic bulky organic A-site cations, which results in the formation of layered halide perovskite (LHP) structures that are analogous to Ruddlesden-Popper phases.[14-16] The LHPs have a chemical formula of $R'_2R_{n-1}B_nX_{3n+1}$, where R', and R represent bulky and small A-site cations, B and X are as defined above, and n represents the number of corner-sharing metal halide $(BX_6)^{4-}$ octahedra sheets that are sandwiched between R' cations, assembling into two-dimensional sheets.[14, 16-19] The inorganic sheets act as free-standing quantum wells that are electronically insulated by bulky organic cations; this results in quantum confined-structures with thickness-tunable optoelectronic properties.[14, 17] Various methods have been used to synthesize LHP single crystals and thin films,[20-22] with proof-of-concept solar cells demonstrating ~15% PCE and improved stability against moisture.[23-26]

Despite improvements in moisture stability through incorporation of bulky organic cations, many LHPs are synthesized with methylammonium (MA), which is a small cation used in high-efficiency Pb-halide perovskites.[27, 28] It has been shown that when perovskites containing MA are exposed to elevated temperatures, CH_3NH_2 is evolved,[10, 11, 29] destroying the desirable electronic properties.[11, 13] This has motivated researchers to replace the MA cation with similarly-sized non-volatile inorganic cations such as Cs. However, the desired cubic perovskite phase of $CsPbI_3$ (α-$CsPbI_3$) is metastable at temperatures below ~330°C,[30-32] and readily transforms to a non-perovskite "yellow phase" (δ-$CsPbI_3$) under ambient conditions.[33-36] The instability of α-$CsPbI_3$ poses a challenge for fabricating stable devices from α-$CsPbI_3$.

While bulk α-$CsPbI_3$ is phase-unstable under ambient conditions, there is growing evidence that size- and surface effects can alter the phase behavior of $CsPbI_3$.[34, 37-39] Eperon and

coworkers determined that α-$CsPbI_3$ thin films with grain sizes on the order of 100 nm have enhanced stability.[34] Colloidal nanocrystals of α-$CsPbI_3$ are stable for at least several days.[40] These results demonstrate that nanostructuring can act as a route to stable α-$CsPbI_3$ devices. Recently, there have been attempts to reduce the dimension of α-$CsPbI_3$ by fabricating LHPs.[41-44] Despite some progress in stability, the layered $R'_2Cs_{n-1}Pb_nX_{3n+1}$thin films have had extremely broad distributions of the layer thickness in LHPs (i.e. a broad distribution in n). This broad distribution is expected to be detrimental to charge carrier transport by introducing a source of energy disorder and reducing the achievable open circuit voltage.[45-48]

In this article, we demonstrate that the use of solvents with high complexation strength can result in intermediate phases that decompose slowly and achieve layered $(C_4H_9NH_3)_2CsPb_2I_7$ ($C_4H_9NH_3$ = BA) thin films with unprecedented stability and narrow distribution in layered perovskite phases. The strongly complexing solvents form solvent:iodoplumbate complexes that are visibly distinct intermediates that remain after spin-coating. This intermediate phase decomposes slowly, which is thought to slow nucleation of LHP crystallites during the processing of these LHP thin films. We demonstrate that processing conditions such as the solution temperature during deposition as well as the annealing conditions can impact the crystallinity and phase purity of these materials. We found that $BA_2CsPb_2I_7$ thin films that were processed using a tetrahydrothiophene 1-oxide (THTO) solvent additive had superior phase stability, both at ambient conditions and at high relative humidity (RH). We also observed improvements in film morphology when using highly-complexing solvent additives, including a reduction in pinhole defects and an increase in grain sizes. We improved the monodispersity of these films by using a temperature ramping method during the annealing process. Furthermore, we found that the layered $BA_2CsPb_2I_7$ thin films can be processed at substantially lower temperatures compared to bulk α-$CsPbI_3$-based thin films, which could make this approach more suitable for applications where flexible or polymeric substrates are desired.

RESULTS AND DISCUSSION

To synthesize $BA_2Cs_{n-1}Pb_nI_{3n+}1$ (schematic in Figure 1a), stoichiometric amounts of n-butylammonium iodide (BAI), PbI_2, and CsI were dissolved in dimethylformamide (DMF) to a total salt concentration of 30 wt. %. It is established that thin films with a targeted value of n > 1 can undergo a structural disproportionation into a broad distribution of n values;[23, 24, 49, 50] thus, the targeted and actual layer thicknesses can differ from each other. Therefore, for clarification, we exclusively refer to "n_{target}" as the product obtained from solutions containing stoichiometric amounts of precursors corresponding to the chemical formula $BA_2Cs_{n-1}Pb_nI_{3n+1}$, while "n" is used exclusively for the pure phase corresponding to a chemical formula of $BA_2Cs_{n-1}Pb_nI_{3n+1}$ (see Table S1, for details).

The absorbance spectra of spin-coated films from precursors dissolved in DMF with n_{target} = 1, 2, 3, and 4 all exhibit a characteristic absorption peak at 511 nm (Figure 1b), which is attributed to the first excitonic transition corresponding to n = 1.[16] Samples with $n_{target} \geq 2$ reveal substantial contributions from phases corresponding to $1 \leq n \leq 3$. The absorption peaks at 548 and 591 nm are attributed to n = 2 and 3, respectively, similar to previous reports on cesium and methylammonium lead iodide LHPs .[24, 42] Furthermore, the broad absorption tail that extends nearly to the band edge of bulk α-$CsPbI_3$ (~715 nm)[31] indicates that these samples also contain impurities of $n \geq 4$. Polydispersity of LHP thin films has been well-documented in several other reports of methylammonium lead iodide-based LHPs.[23, 24, 50, 51] Thin films with high enough concentrations of Cs ($n_{target} \geq 3$) favor the formation of δ-$CsPbI_3$ and exhibit absorbance features that correspond primarily to n = 1, and δ-$CsPbI_3$. Because of the perceived challenge of synthesizing $BA_2Cs_{n-1}Pb_nI_{3n+1}$ with $n \geq 3$, the focus in this article is films with n_{target} = 2.

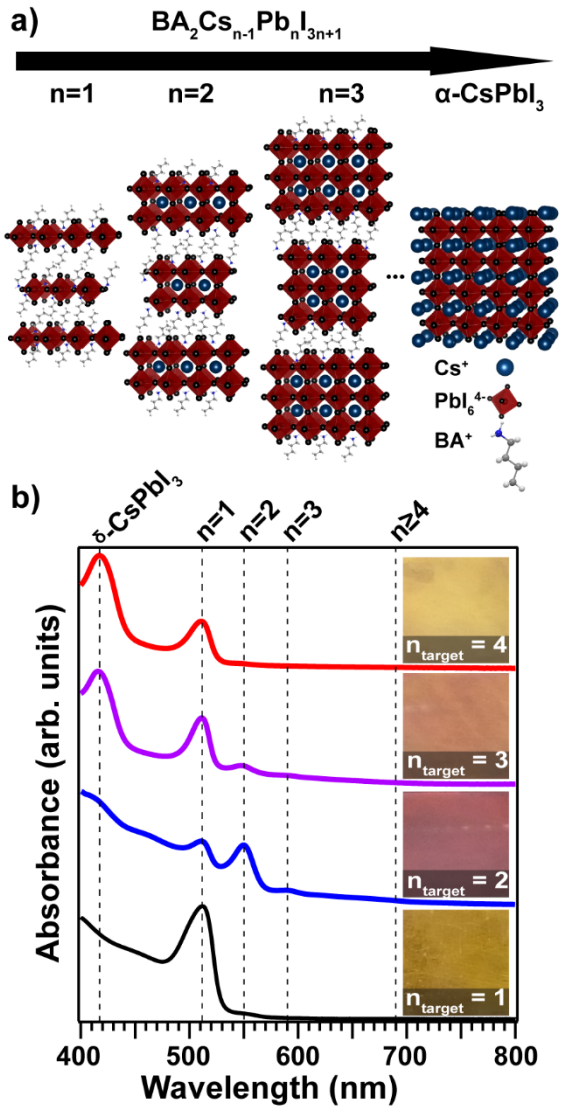

Figure 1. a) Schematic of layered $BA_2Cs_{n-1}Pb_nI_{3n+1}$ (n = 1, 2, 3, and α-$CsPbI_3$), and b) Absorbance spectra of n_{target} = 1, 2, 3, and 4 thin films prepared from neat DMF with respective photographs. Absorbance spectra are calculated from transmittance spectra.

In an initial effort to synthesize n_{target} = 2 thin films with improved phase purity, we studied the effects of solution temperature. We found that dissolving the precursors in a warm (~65 °C) DMF solution prior to spin-coating resulted in a substantial

increase in the intensity of the absorbance peak associated with n = 2 (see Figure S1). It is known that Cs salts have low solubility in DMF,[41] and the increased temperature could improve solubility of CsI during deposition, resulting in a more monodisperse compositional profile during spin-coating and encouraging crystallization of n = 2. Alternatively, heating could also affect the solvated PbI_2 as it is known that PbI_2 can exist as relatively large colloidal particles in solutions of DMF; heating could potentially aid in the dissolution of these particles.[52, 53] Although heating the precursor solution increased the monodispersity, the absorbance spectra also featured substantial contributions from the n = 1 and n = 3 phases.

We hypothesized that the polydispersity could also arise from poor control over the nucleation and crystal growth during spin-coating. It was found that slowing down the nucleation resulted in improved monodispersity in $BA_2MA_{n-1}Pb_nI_{3n+1}$ LHPs.[54] We sought to slow the nucleation and growth process in our system by adding complexing solvents to the precursor solutions that have high affinity towards Pb^{2+}.[55, 56] As a metric for complexing strength, we used the Gutmann donor number (DN),[57] which has been used in previous studies to describe the effects of complexation strength in $MAPbI_3$.[58] We chose multiple solvents with a high DN including dimethylacetamide (DMAC)), n-methyl-2-pyrrolidone (NMP), N,N′-dimethylpropyleneurea (DMPU), dimethylsulfoxide (DMSO), and THTO ; (see Table 1 for solvent properties). Although the DN is not determined for THTO, computational and experimental studies show that THTO has strong solvation and coordination ability[54, 59, 60] with a DN similar to tetrathiourea (see Supporting Information for details).

Table1: Solvent properties including DN, boiling point, and vapor pressure for DMF, and additive solvents. DN was adapted from[61].

O C S H N						
Solvent	DMF	DMAC	NMP	DMSO	DMPU	THTO
Donor type	O	O	O	O	O	O
Boiling point (°C)	153	165	202	189	146	236
DN (kcal.mol^{-1})	26.6	27.8	27.3	29.8	33.0	~30.0 (estimated)
Vapor pressure	2.70	2.00	0.29	0.42	0.37	N.A.

These high DN solvents were added in different amounts in the precursor solution (See Table S2) and heated to 65 °C prior to spin-coating deposition which was followed by thermal annealing at 100 ± 5 °C. Samples prepared with neat DMF are referred to by "DMF-method", while those prepared with multiple solvents are referred to by the complexing solvent (e.g. THTO-method, NMP-method, etc.). It should be noted that in all methods, thin films were immediately thermally annealed after spin-coating unless stated otherwise. We observed that the inclusion of solvents with high DN in the solutions with n_{target} = 2 had a dramatic effect on the nucleation dynamics (see Movie S1). As shown in the Movie S2, NMP-method films with a 2:1 molar ratio of NMP:Pb were transparent yellow immediately after spin-coating. Within 15 seconds of keeping the film at a temperature of 40 ± 5 °C, the film color transformed to dark red-orange. In contrast, THTO-method films with a 1:1 molar ratio of THTO: Pb underwent this transition much more slowly, transitioning from transparent yellow to light orange after ~10 minutes at 40 ± 5 °C. It was observed that THTO-method films (Movie S3) needed longer time and elevated temperature for complete crystallization compared to DMF-method films (Movie S4). The observed difference in the transformation dynamics can be used to gain insight to the interplay of precursor decomposition, crystal nucleation, and growth processes. The rapid color change that occurs in NMP-method films implies that the precursor decomposes rapidly, forming a high density of nuclei on the substrate; supersaturation of nuclei promotes faster crystal growth within the film,[62, 63] supporting faster growth in NMP-method films. In contrast, the slower color change that is observed in THTO-method films can be attributed to slower crystal nucleation. It has been previously demonstrated that THTO can dramatically slow crystallite nucleation in bulk and methylammonium lead iodide LHP thin films,[54, 59] which is similar to what we visually observed in our films. The absorbance spectra (Figure 2a, and S2) of n_{target} = 2 thin films demonstrate that in all cases, using high DN solvents resulted in enhanced monodispersity; the characteristic peak for the n = 2 phase at 548 nm was enhanced, while the peaks corresponding to n = 1 and n = 3 phases were suppressed. All n_{target} = 2 thin films were stable for at least eight months in a glovebox filled with N_2. When exposed to air, the phase stability of the n_{target} = 2 thin films was found to depend on the choice of complexing solvent used in the precursor solution. Films prepared with DMF- and DMAC-methods did not show high stability at ambient conditions at low RH. The thin films prepared by both methods turned to n =1 and δ-$CsPbI_3$ after being exposed to RH of ~ 20-30 % (Figure S3) in 5 days, while other thin films were stable. In another sets of experiments, we exposed thin films to RH ~ 45%. By increasing RH, DMSO-method films also lost the stability in 5 days (Figure S4) and some small yellow spots appeared in NMP-method film. Films deposited by the NMP-method (which had the narrowest distribution in n of all our samples) almost completely transformed to a combination of δ-$CsPbI_3$ and n = 1 after ~5 days at RH ~ 55%, while films prepared by the THTO-method consistently retained their phase under the same conditions (Figure 2b, and c). Top view scanning electron microscopy (SEM) revealed that using the THTO-method resulted in more compact films with fewer pinhole defects (inset Figure 2d). In contrast, films processed using the NMP-method featured micron-sized isolated grains with large amounts of void space (inset Figure 2e). Cross sectional SEM images (Figure 2d, and e) indicate thicker, and more dense film morphology for THTO-method compared to NMP-method. The undesirable morphology of these films likely originates from the rapid and poorly-controlled crystallization process in thin films,[62] which is in line with previous studies that demonstrate improved morphologies through the use of complexing solvents which form intermediate complexes that decompose slowly.[54, 56, 58, 59, 64-66] We suspect that poor morphology of films prepared using the NMP-method results in infiltration of atmospheric moisture, which is known to catalyze the phase transformation from α-$CsPbI_3$ to δ-$CsPbI_3$, resulting in lower stability.[34]

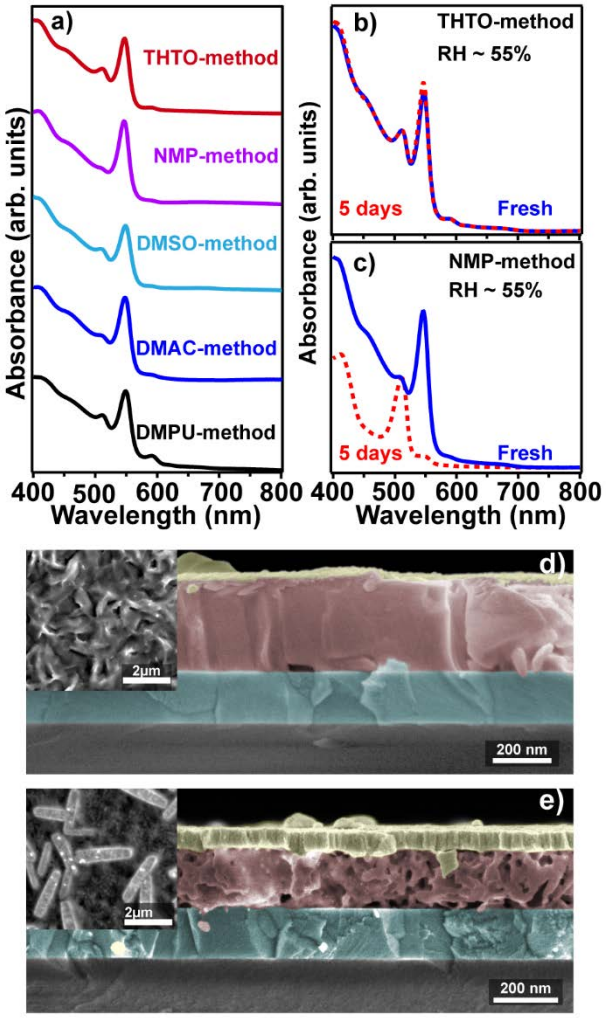

Figure 2: a) Absorbance spectra of n_{target} = 2 thin films with optimized molar ratio for THTO, NMP, DMSO, DMAC, and DMPU additives, b), and c) Stability test of n_{target} = 2 at RH~ 55% with 1 THTO: 1 Pb and 2 NMP: 1 Pb, respectively, d), and e) Cross sectional scanning electron microscopy (SEM) of fresh n_{target} = 2 thin films prepared with 1 THTO: 1 Pb, and 2 NMP: 1 Pb, respectively. Insets in d), and e) are top-view SEM images. Absorbance spectra are calculated from the transmittance spectra of thin films.

To assess the stability of the films against moisture, we placed n_{target} = 2 films fabricated with the THTO method in an environment containing different RHs (Figure 3). We exposed films for 3 weeks to a RH of ~20%, after which the films were exposed to a RH of ~75%. Absorbance spectra after 5 months demonstrate some features of δ-$CsPbI_3$, however the stability is apparent through the persistent dominance of the n = 2 peak; this stability is still observed after 8 months. In contrast, we exposed films immediately to elevated RH, and subsequently observed decomposition to n = 1 and δ-$CsPbI_3$ within ~6 hours. These results imply that enhanced stability can be obtained by exposure to controlled humidity level for LHPs, and this stability could be further improved through optimization of the processing conditions.

Encouraged by the long-term stability of n_{target} = 2 thin films prepared by THTO-method, we focused on further improving

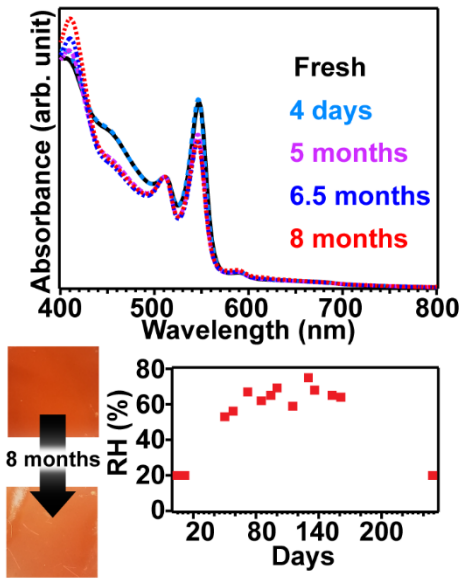

Figure 3: Absorbance spectra of THTO-method film exposed to various RH level over time. All spectra are normalized to excitonic feature at 511 nm corresponding to n = 1. Absorbance spectra are calculated based on transmittance spectra.

the monodispersity in these samples. We hypothesized that gradually increasing the annealing temperature would further slow down the decomposition of the intermediate phase, thereby further improving the monodispersity of the thin films (Schematic 1). We applied a temperature ramp to the films by placing the spin-coated substrate on a hotplate set at 40 ± 5 °C and raised the temperature to 100 ± 5 °C at a rate of ~1 °C/min (THTO-Ramp-method). We observed that by using the THTO-Ramp-method, the absorbance peak corresponding to n = 1 (511 nm) was completely suppressed, and the peak intensities for n ≥ 3 were substantially reduced (Figure 4a, and Figure

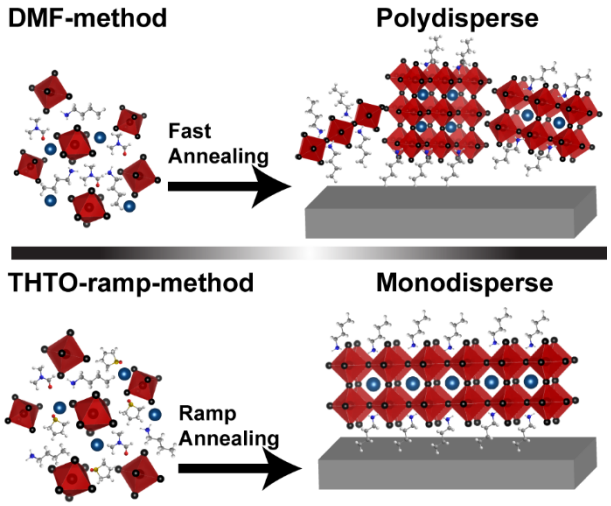

Schematic 1: Illustration of intermediate phase decomposition by DMF-method and THTO-ramp-method

S5). Top view SEM images (Figure 4b) of THTO-Ramp-method films show a more uniform film morphology compared to the films without temperature ramping. These films showed very good stability at a RH ~ 20-30% (Figure S6a) for 5-days, but they lost their stability upon exposure to RH ~ 45% (Figure S6b). Although, top view SEM image indicates compact film morphology, cross sectional SEM image (Figure S6c) indicates layered structure with non-uniform film thickness. As mentioned earlier, poor surface morphology could result in the instability of the films. We believe that further investigation would be useful to understand the effect of surface morphology on the stability of LHP thin films. We performed similar preliminary studies for n_{target} = 3, and 4. However, the thin films still were polydisperse with low stability (Figure S7).

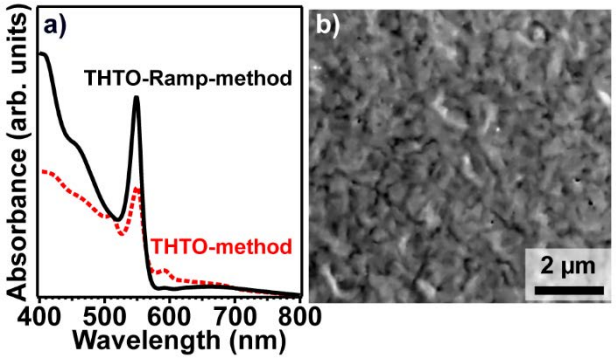

Figure 4: a) Absorbance spectra of n_{target} = 2 thin film prepared by THTO-Ramp-method and THTO-method, and b) SEM image of n_{target} = 2 film by THTO-Ramp-method. Absorbance spectra are calculated based on transmittance spectra.

To better understand the effects of adding highly complexing solvents on the structure of these thin films, we acquired X-ray diffraction (XRD) patterns of n_{target} = 1 and 2 thin films. For the n_{target} = 1 film, reflections were observed at 2θ = 6.46, 12.86, 19.31, 25.82, and 32.42 °, corresponding to the (002), (004), (006), (008), and (0010) planes, respectively (Figure S8). The prominence of these diffraction peaks indicate that the sheets are oriented parallel to the substrate which is common for many 2D materials.[67] For the n_{target} = 2, we noted that the thin film prepared by DMF-method (Figure 5) had very weak diffraction, and broad features that imply a lack of crystallinity. In contrast, films deposited by NMP- and THTO-methods had much stronger diffractions, indicating that these films had a greater degree of long-range order. In the case of NMP-method, a low-intensity reflection was observed at 4.5 ° which corresponds to the (002) plane of n = 2 phase. Additional peaks observed at 14.41 and 28.70° correspond to (100), and (200) reflections in the n = 2 phase.[42, 68] The lack of additional peaks imply that the structure of the sheets do not feature octahedral tilting similar to the β-$CsPbI_3$ structure, but rather the cubic symmetry of the α-$CsPbI_3$[34] structure. In the case of THTO-method, we observed the pattern is comprised of a combination of n = 1, n = 2, and α-$CsPbI_3$, agreeing well with the absorbance results, indicating that this sample is polydisperse. Thin films prepared by THTO-Ramp-method had a markedly different diffraction pattern compared to films prepared by THTO-method. The presence of high order {001} diffraction peaks for n_{target} = 2 thin film with THTO-Ramp-method indicates that these well-crystallized perovskite sheets are oriented parallel to the substrate (Figure 5

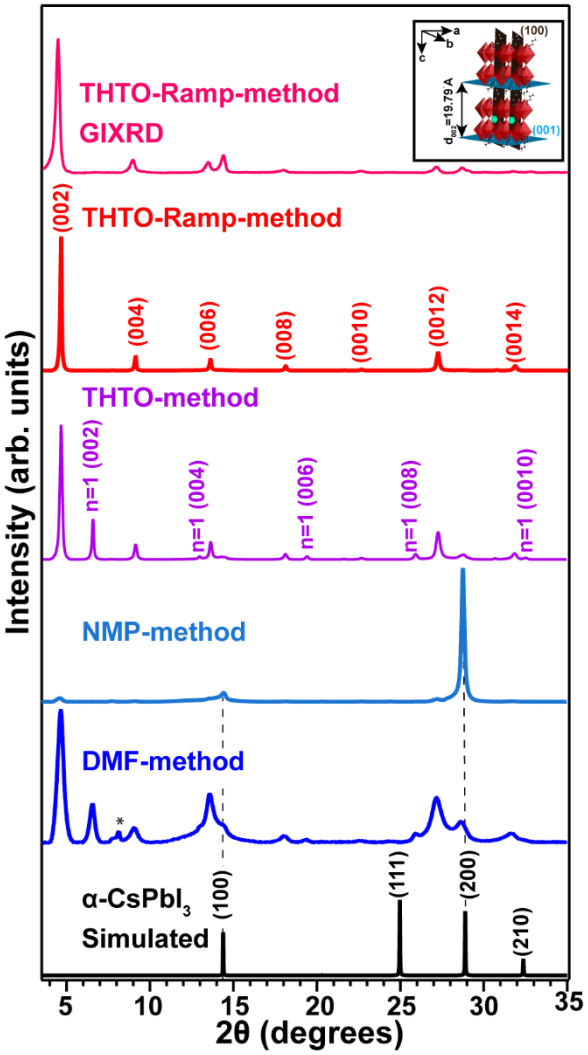

Figure 5: Thin film XRD pattern of simulated α-$CsPbI_3$ (black)[68], n_{target} = 2 by DMF-method (blue), NMP-method (light blue), THTO-method (purple), THTO-Ramp-method (red), and GIXRD of THTO-Ramp-method (pink). Inset schematic illustrates the LHPs orientation. Dashed line is used to guide the eye. * indicates diffraction peak from substrate holder.

inset).[67] In addition, the absence of diffraction pattern from{100} planes in the gonio scan and the presence of peaks-belonging to the (100) and (200) planes in the grazing incident XRD (GIXRD) measurements provides additional evidence that the sheets are oriented parallel to the substrate. It is important to note that the [100] direction in α-$CsPbI_3$ is equivalent to the [100] direction in the simulated n = 2 structure (Figure S8). The absence of peaks at 2θ = 6.46, 3.40 or 2.76 ° and their multiples (which correspond to the {001} for n = 1, 3, and 4, respectively) indicate that only the n = 2 phase is observed. Furthermore, an elongation of the c-axis from 27.3 Å for n = 1 to 39.6 Å for n = 2 is in good agreement with the addition of two α-$CsPbI_3$ layers (~6.17 Å) per unit cell,[34, 67, 69] further confirming the prevalence of n = 2 phase. We performed grazing incident wide angle x-ray scattering (GIWAXS) measurements to

confirm the orientation of the LHP thin films. As shown in Figure 6, the THTO-, and THTO-Ramp-methods samples are oriented parallel to the substrate with the highest intensity peaks along Q_z. The strong scattering peak observed at Q_z = 0.32 Å corresponds to the (002) plane for n = 2 species, and it is in a good agreement with our 1D XRD pattern. The presence of higher order {00l} reflections also confirmed in our GIWAXS data. The THTO-method sample showed impurities from n =1 phases which are also oriented parallel to the substrate. However, we did not observe any scattering peaks from n = 1 phases in the THTO-Ramp-method. Both samples had scattering peaks with relatively low intensity from α-$CsPbI_3$ with (100), and (200) planes (See Figure S9 for full size images).

Our efforts in reducing the polydispersity of layered perovskites were motivated by improving the performance of solar cells that use layered perovskite thin films, since polydispersity

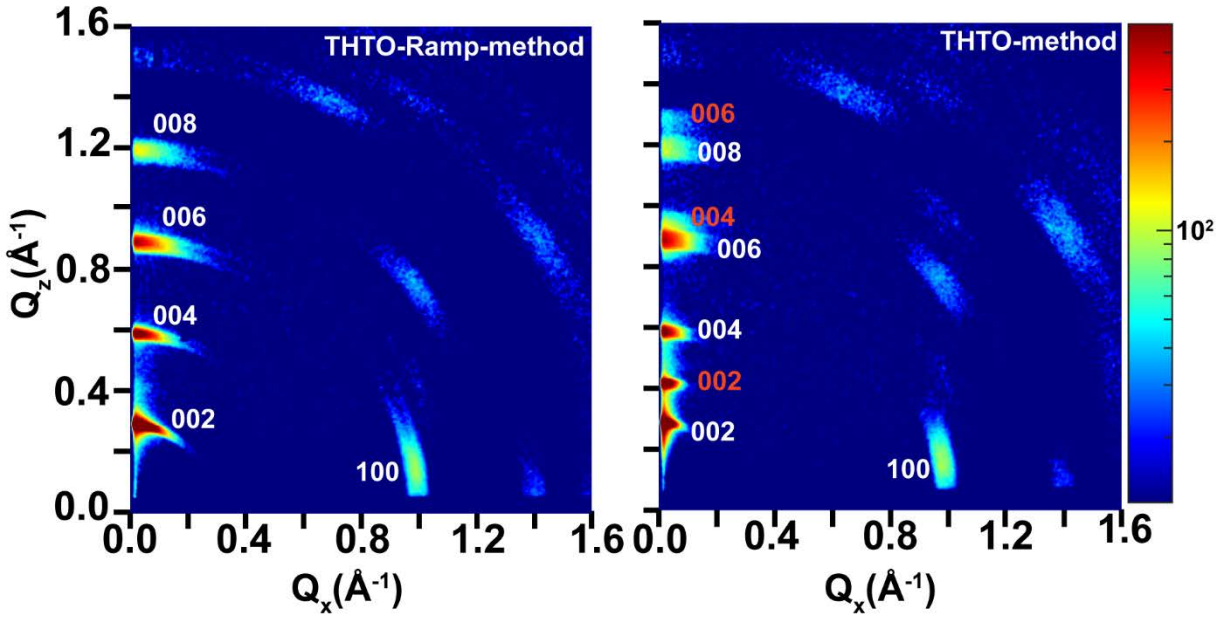

Figure 6: Grazing incident wide angle X-ray scattering (GIWAXS) of THTO-, and THTO-Ramp-method thin films. Indices in orange represent n = 1, and white represent n = 2 phases.

introduces a site-energy distribution that would be expected to negatively impact the performance.[70, 71] The site-energy distribution has previously been described using photoluminescence (PL).[71] We obtained room temperature PL spectra of n_{target} = 2 processed by DMF-, NMP- and THTO-Ramp-methods. As shown in Figure 7 and Figure S10a, several excitonic features were observed for all samples implying the presence of different n layer thicknesses. However, the peak observed for n_{target} = 2 in thin films prepared from neat DMF was weak and the PL intensity was dominated by values of n ≥ 3. This could be explained by energy transfer to lower energy states.[43] For NMP-method the dominant peak was observed for n = 3 phase (Figure S10a), although, the absorbance was dominated by n = 2 phase (Figure S10b). In the more monodisperse sample of THTO-Ramp-method, PL was primarily associated with the n = 2 species, likely because there are relatively few lower-energy states to which energy can transfer. Conversely, in the polydisperse sample there are many different energy states that are proximal to each other, facilitating a PL spectrum that is dominated by the lowest-energy states. THTO-Ramp-method results show that reducing the distribution n of energetic states could effectively reduce the number of traps in the system, and improve charge transport.

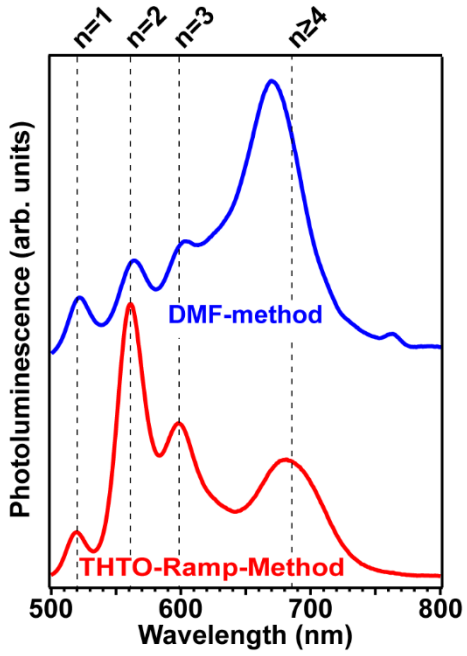

Figure 7: Room temperature photoluminescence of n_{target} = 2 thin films prepared from DMF-method and THTO-Ramp-method.

CONCLUSION

In this work, we investigated the effect of adding complexing solvents to precursor solutions on the crystallization dynamics of layered $BA_2CsPb_2I_7$ LHP thin films. The presence of additive solvents with strong Pb^{2+} complexation was found to enhance the monodispersity. Incorporating the additive solvents in the precursor solutions controlled the decomposition of intermediate phases, which is believed to affect the nucleation rate and subsequent crystal growth. It is shown that for $BA_2CsPb_2I_7$, slower decomposition of the intermediate phase is achieved by using high complexing THTO additive solvent, followed by gradual increase in annealing temperature named as Ramp-method, and this resulted in stable, monodisperse thin films with compact film morphology. The films with an orientation parallel to the substrate showed pha e stability over several months in ambient conditions. In contrast, using NMP as an additive in the precursor solution of $BA_2CsPb_2I_7$ resulted in faster intermediate phase decomposition during annealing as represented by a quick color change, resulting in films with a preferential orientation correspond to α-$CsPbI_3$. However, these films exhibited poor surface morphology and substantially lower stability when exposed to ambient conditions. The long-term stability of thin films prepared with THTO additives suggest their potential applications in electronic devices such as FETs where the parallel orientation to the substrate is preferred.

MATERIALS AND METHODS

PbI_2 (TCI, 99.99%, trace metal basis), BAI (Greatcell solar), CsI (Sigma-Aldrich, 99.999%, trace metal basis), DMF (Sigma-Aldrich, 99.8%, anhydrous), THTO (Sigma-Aldrich, 96%), NMP (Sigma-Aldrich, 99.5%, anhydrous), DMAC (Sigma-Aldrich, 99.8%, anhydrous), and DMPU (Sigma-Aldrich, 98%) were all used without further purification. Indium tin oxide (ITO) substrates (25 mm x 25 mm) were purchased from Thin Film Devices.

Substrate preparation: All substrates including bare glass and ITO were cleaned as follows prior to solution deposition. All substrates were sonicated in detergent and Millipore DI water bath for 10 min, rinsed with a copious amount of Millipore DI water and sonicated in Millipore DI water for 10 min. Substrates were then cleaned with sonication in acetone and isopropanol, each for 10 min, and dried with N_2 gun flow. At the end, substrates were O_2 plasma cleaned (Harrick Plasma, PDC-001-HP) for 15 min at high and transferred to the glovebox filled with N_2.

Solution synthesis and thin film fabrication of layered $BA_2Cs_{n-1}Pb_nI_{3n+1}$ perovskites: $BA_2Cs_{n-1}Pb_nI_{3n+1}$, (n = 1, 2, 3, and 4) precursor solutions were synthesized by dissolving stoichiometric amounts of PbI_2, CsI, and BAI in DMF at room temperature to get the total concentration of 30 wt.% (amounts are tabulated in Table S1) to obtain optically clear yellow solution. In the case of n_{target} = 2 with additive solvent, various molar ratios of additive solvents to Pb atom was used during the solution preparation to get the total concentration of 30 wt.%. It should be noted that the precursors were measured first, then the additive solvent and consequently DMF solvent was added to the precursors. The solutions then were heated at 65 °C for at least 30 minutes, creating an optically clear yellow solution. To create thin films, 100 µl of warm precursor solution was dispensed using a 1000 µl pipette (Eppendorf) onto a clean 25 x 25 mm substrate. These films were spin-coated at 4000 rpm for 40s, followed by two different thermal annealing processes named as fast and ramp annealing.

Fast annealing: substrates were immediately placed on an aluminum block on a hotplate where the actual temperature was 100 ± 5 °C after spin-coating and annealed for ~ 10 min.

Ramp annealing: substrates were placed on an aluminum block on a hotplate set at 50°C (actual temperature = 40 ± 5 °C). The temperature was manually increased by 10 °C/10 min to reach 140 °C (actual temperature = 100 ± 5 °C).

Characterization and data analysis: XRD and GIXRD patterns for thin films were obtained using Bruker DaVinci D8 Advance diffractometer equipped with a Cu Kα radiation source with 1D/0D detector. GIWAXS data were obtained using Xenocs Xeuss 2.0 SWAXS. The system is set with monochromatized X-ray using Mo Kα radiation of the wavelength 07107 Å. Data were collected by Pilatus 1M detector at the sample to detector distance of 364.397 mm calibrated by silver behenate standard. The acquisition was 36000 s with the incident x-ray angle of 0.35°. Image data were processed by Foxtrot software.

UV-Vis absorption spectra were acquired using PerkinElmer Lambda 750 spectrophotometer equipped with a labsphere100 mm integrating sphere in transmittance mode. The coated samples on microscope glass slide were placed in front of the light source and the data were collected in the range of 400- 800 nm. Steady-state fluorescence spectra (PL) were obtained on a Fluoromax-4 spectrometer (Horiba Scientific) and corrected for lamp spectral intensity and detector response. A thin film of the sample, coated on glass, was placed inside the sample compartment in a front-faced geometry with the sample side facing the excitation light and the detector. The band-widths for the excitation and the emission were set to 10 nm. The sample was excited at 450 nm with vertically polarized light and emission was collected in the 500-800 nm range by setting a polarizer in the horizontal direction. A 490 nm long-pass filter was used to eliminate scattered light. Scanning electron microscopy images in top-view and cross sectional modes were imaged near the center of samples using FEI Teneo Lovac FE-SEM with an accelerating voltage of 5k, and FEI Helios Nanolab Dual-Beam, respectively.

ASSOCIATED CONTENT

Supporting Information

This material is available free of charge via the Internet at http://pubs.acs.org

Details on data analysis, and THTO DN calculation; Tables for solution synthesis, and processing conditions; Optical absorbance data; stability tests, XRD pattern for n_{target} = 1 and simulated n = 2; full size GIWAXS data; cross sectional SEM image of THTO-Ramp-method; PL of NMP-method; and videos of film processing.

AUTHOR INFORMATION

Corresponding Author

* Email address: panthani@iastate.edu

Author Contributions

The manuscript was written through contributions of all authors. All authors have given approval to the final version of the manuscript.

Notes

The authors declare no competing financial interest.

ACKNOWLEDGMENT

The authors would like to thank Matt Besser from Ames laboratory for assistance in acquiring XRD measurements, Dr. Matthew Lynn for assisting us in imaging cross sectional SEM of thin films, Dr. Jake W. Petrich for allowing access to the Fluoromax-4 spectrometer, and Alireza Saraeian for useful discussions during the experimental design. Authors acknowledge support from Division of Material Research NSF-DMR for funding the SAXS instrument under Grant Number (NSF-DMR-1626315). AH acknowledges support from the Catron Foundation. BJR and RDN acknowledge funding support from the National Science Foundation Graduate Research Fellowship Program under Grant Number (DGE 1744592). KS acknowledges funding support from the U.S. Department of Energy (DOE) Ames Laboratory, which is operated for the U.S. DOE by Iowa State University under contract Number DE-AC02-07CH11358. MGP acknowledges support from the Herbert L. Stiles Faculty Fellowship. This research was partially supported by the AFOSR Young Investigator Program, under Grant # FA9550-17-1-0170.

REFERENCES

1. Stranks, S. D.; Eperon, G. E.; Grancini, G.; Menelaou, C.; Alcocer, M. J. P.; Leijtens, T.; Herz, L. M.; Petrozza, A.; Snaith, H. J., Electron-hole diffusion lengths exceeding 1 micrometer in an organometal trihalide perovskite absorber. *Science* **2013,** 342, 341-344.

2. Xing, G.; Mathews, N.; Sun, S.; Lim, S. S.; Lam, Y. M.; Grätzel, M.; Mhaisalkar, S.; Sum, T. C., Long-range balanced electron- and hole-transport lengths in organic-inorganic $CH_3NH_3PbI_3$. *Science* **2013,** 342, 344-347.

3. Dong, Q.; Fang, Y.; Shao, Y.; Mulligan, P.; Qiu, J.; Cao, L.; Huang, J., Electron-hole diffusion lengths> 175 μm in solution grown $CH_3NH_3PbI_3$ single crystals. *Science* **2015**, 347, 967-970.

4. Correa-Baena, J.-P.; Saliba, M.; Buonassisi, T.; Grätzel, M.; Abate, A.; Tress, W.; Hagfeldt, A., Promises and challenges of perovskite solar cells. *Science* **2017,** 358, 739-744.

5. McMeekin, D. P.; Sadoughi, G.; Rehman, W.; Eperon, G. E.; Saliba, M.; Hörantner, M. T.; Haghighirad, A.; Sakai, N.; Korte, L.; Rech, B., A mixed-cation lead mixed-halide perovskite absorber for tandem solar cells. *Science* **2016,** 351, 151-155.

6. Miyasaka, T., Lead Halide Perovskites in Thin Film Photovoltaics: Backgrounds and Perspectives. *Bull. Chem. Soc. Jpn.* **2018**, 91, 1058-1068.

7. Lin, Q.; Armin, A.; Nagiri, R. C. R.; Burn, P. L.; Meredith, P., Electro-optics of perovskite solar cells. *Nat. Photonics* **2015,** 9, 106-112.

8. Fu, Y.; Meng, F.; Rowley, M. B.; Thompson, B. J.; Shearer, M. J.; Ma, D.; Hamers, R. J.; Wright, J. C.; Jin, S., Solution growth of single crystal methylammonium lead halide perovskite nanostructures for optoelectronic and photovoltaic applications. *J. Am. Chem. Soc.* **2015,** 137, 5810-5818.

9. Best Research-Cell Efficiency Chart. https://www.nrel.gov/pv/cell-efficiency.html (June 3rd, 2019).

10. Conings, B.; Drijkoningen, J.; Gauquelin, N.; Babayigit, A.; D'Haen, J.; D'Olieslaeger, L.; Ethirajan, A.; Verbeeck, J.; Manca, J.; Mosconi, E., Intrinsic thermal instability of methylammonium lead trihalide perovskite. *Adv. Energy Mater.* **2015,** 5, 1500477.

11. Han, Y.; Meyer, S.; Dkhissi, Y.; Weber, K.; Pringle, J. M.; Bach, U.; Spiccia, L.; Cheng, Y.-B., Degradation observations of encapsulated planar $CH_3NH_3PbI_3$ perovskite solar cells at high temperatures and humidity. *J. Mater. Chem. A* **2015,** 3, 8139-8147.

12. Berhe, T. A.; Su, W.-N.; Chen, C.-H.; Pan, C.-J.; Cheng, J.-H.; Chen, H.-M.; Tsai, M.-C.; Chen, L.-Y.; Dubale, A. A.; Hwang, B.-J., Organometal halide perovskite solar cells: degradation and stability. *Energy Environ. Sci.* **2016,** 9, 323-356.

13. Christians, J. A.; Miranda Herrera, P. A.; Kamat, P. V., Transformation of the Excited State and Photovoltaic Efficiency of $CH_3NH_3PbI_3$ Perovskite upon Controlled Exposure to Humidified Air. *J. Am. Chem. Soc.* **2015,** 137, 1530-1538.

14. Mitzi, D. B.; Feild, C. A.; Harrison, W. T. A.; Guloy, A. M., Conducting tin halides with a layered organic-based perovskite structure. *Nature* **1994,** 369, 467-469.

15. Mitzi, D. B., Templating and structural engineering in organic–inorganic perovskites. *J. Chem. Soc., Dalton Trans.* **2001**, 1-12.

16. Stoumpos, C. C.; Cao, D. H.; Clark, D. J.; Young, J.; Rondinelli, J. M.; Jang, J. I.; Hupp, J. T.; Kanatzidis, M. G., Ruddlesden–Popper hybrid lead iodide perovskite 2D homologous semiconductors. *Chem. Mater.* **2016,** 28, 2852-2867.

17. Mitzi, D. B., Synthesis, Crystal Structure, and Optical and Thermal Properties of $(C_4H_9NH_3)_2MI_4$ (M= Ge, Sn, Pb). *Chem. Mater.* **1996,** 8, 791-800.

18. Cao, D. H.; Stoumpos, C. C.; Farha, O. K.; Hupp, J. T.; Kanatzidis, M. G., 2D homologous perovskites as light-absorbing materials for solar cell applications. *J. Am. Chem. Soc.* **2015,** 137, 7843-7850.

19. Cao, D. H.; Stoumpos, C. C.; Yokoyama, T.; Logsdon, J. L.; Song, T.-B.; Farha, O. K.; Wasielewski, M. R.; Hupp, J. T.; Kanatzidis, M. G., Thin Films and Solar Cells Based on Semiconducting Two-Dimensional Ruddlesden-Popper $(CH_3(CH_2)_3NH_3)_2(CH_3NH_3)_{n-1}Sn_nI_{3n+1}$ Perovskites. *ACS Energy Lett.* **2017,** 2, 982-990

20. Takeoka, Y.; Fukasawa, M.; Matsui, T.; Kikuchi, K.; Rikukawa, M.; Sanui, K., Intercalated formation of two-dimensional and multi-layered perovskites in organic thin films. *Chem. Commun.* **2005**, 378-380.

21. Era, M.; Hattori, T.; Taira, T.; Tsutsui, T., Self-organized growth of PbI-based layered perovskite quantum well by dual-source vapor deposition. *Chem. Mater.* **1997,** 9, 8-10.

22. Koh, T. M.; Shanmugam, V.; Schlipf, J.; Oesinghaus, L.; Müller-Buschbaum, P.; Ramakrishnan, N.; Swamy, V.; Mathews, N.; Boix, P. P.; Mhaisalkar, S. G., Nanostructuring Mixed-Dimensional Perovskites: A Route Toward Tunable, Efficient Photovoltaics. *Adv. Mater.* **2016,** 28, 3653-3661.

23. Smith, I. C.; Hoke, E. T.; Solis-Ibarra, D.; McGehee, M. D.; Karunadasa, H. I., A layered hybrid perovskite solar-cell absorber with enhanced moisture stability. *Angew. Chem.* **2014,** 126, 11414-11417.

24. Quan, L. N.; Yuan, M.; Comin, R.; Voznyy, O.; Beauregard, E. M.; Hoogland, S.; Buin, A.; Kirmani, A. R.; Zhao, K.; Amassian, A., Ligand-stabilized reduced-dimensionality perovskites. *J. Am. Chem. Soc.* **2016,** 138, 2649-2655.

25. Tsai, H.; Nie, W.; Blancon, J.-C.; Stoumpos, C. C.; Asadpour, R.; Harutyunyan, B.; Neukirch, A. J.; Verduzco, R.; Crochet, J. J.; Tretiak, S., High-efficiency two-dimensional Ruddlesden–Popper perovskite solar cells. *Nature* **2016,** 536, 312-316.

26. Zhang, X.; Wu, G.; Yang, S.; Fu, W.; Zhang, Z.; Chen, C.; Liu, W.; Yan, J.; Yang, W.; Chen, H., Vertically Oriented 2D Layered Perovskite Solar Cells with Enhanced Efficiency and Good Stability. *Small* **2017,** 13, 1700611.

27. Ahn, N.; Son, D.-Y.; Jang, I.-H.; Kang, S. M.; Choi, M.; Park, N.-G., Highly reproducible perovskite solar cells with average efficiency of 18.3% and best efficiency of 19.7% fabricated via Lewis base adduct of lead (II) iodide. *J. Am. Chem. Soc.* **2015,** 137, 8696-8699.

28. Yoon, H.; Kang, S. M.; Lee, J.-K.; Choi, M., Hysteresis-free low-temperature-processed planar perovskite solar cells with 19.1% efficiency. *Energy Environ. Sci.* **2016,** 9, 2262-2266.

29. Philippe, B.; Park, B.-W.; Lindblad, R.; Oscarsson, J.; Ahmadi, S.; Johansson, E. M. J.; Rensmo, H., Chemical and Electronic Structure Characterization of Lead Halide Perovskites and Stability Behavior under Different Exposures—A Photoelectron Spectroscopy Investigation. *Chem. Mater.* **2015,** 27, 1720-1731.

30. Hutter, E. M.; Sutton, R. J.; Chandrashekar, S.; Abdi-Jalebi, M.; Stranks, S. D.; Snaith, H. J.; Savenije, T. J., Vapour-Deposited Cesium Lead Iodide Perovskites: Microsecond Charge Carrier Lifetimes and Enhanced Photovoltaic Performance. *ACS Energy Lett.* **2017,** 2, 1901-1908.

31. Liang, J.; Wang, C.; Zhao, P.; Lu, Z.; Ma, Y.; Xu, Z.; Wang, Y.; Zhu, H.; Hu, Y.; Zhu, G., Solution synthesis and phase control of inorganic perovskites for high-performance optoelectronic devices. *Nanoscale* **2017,** 9, 11841-11845.

32. Stoumpos, C. C.; Malliakas, C. D.; Kanatzidis, M. G., Semiconducting tin and lead iodide perovskites with organic cations: phase transitions, high mobilities, and near-infrared photoluminescent properties. *Inorg. Chem.* **2013,** 52, 9019-9038.

33. Stoumpos, C. C.; Kanatzidis, M. G., The renaissance of halide perovskites and their evolution as emerging semiconductors. *Acc. Chem. Res.* **2015,** 48, 2791-2802.

34. Eperon, G. E.; Paternò, G. M.; Sutton, R. J.; Zampetti, A.; Haghighirad, A. A.; Cacialli, F.; Snaith, H. J., Inorganic caesium lead iodide perovskite solar cells. *J. Mater. Chem. A* **2015,** 3, 19688-19695.

35. Chen, C. Y.; Lin, H. Y.; Chiang, K. M.; Tsai, W. L.; Huang, Y. C.; Tsao, C. S.; Lin, H. W., All-Vacuum-Deposited Stoichiometrically Balanced Inorganic Cesium Lead Halide Perovskite Solar Cells with Stabilized Efficiency Exceeding 11%. *Adv. Mater.* **2017,** 29, 1605290.

36. Marronnier, A.; Roma, G.; Boyer-Richard, S.; Pedesseau, L.; Jancu, J.-M.; Bonnassieux, Y.; Katan, C.; Stoumpos, C. C.; Kanatzidis, M. G.; Even, J., Anharmonicity and Disorder in the Black Phases of Cesium Lead Iodide Used for Stable Inorganic Perovskite Solar Cells. *ACS Nano* **2018,** 12, 3477-3486.

37. Zhang, T.; Dar, M. I.; Li, G.; Xu, F.; Guo, N.; Grätzel, M.; Zhao, Y., Bication lead iodide 2D perovskite component to stabilize inorganic α-CsPbI3 perovskite phase for high-efficiency solar cells. *Sci. adv.* **2017,** 3, e1700841.

38. Fu, Y.; Rea, M. T.; Chen, J.; Morrow, D. J.; Hautzinger, M. P.; Zhao, Y.; Pan, D.; Manger, L. H.; Wright, J. C.; Goldsmith, R. H., Selective stabilization and photophysical properties of metastable perovskite polymorphs of $CsPbI_3$ in thin films. *Chem. Mater.* **2017,** 29, 8385-8394.

39. Wang, Q.; Zheng, X.; Deng, Y.; Zhao, J.; Chen, Z.; Huang, J., Stabilizing the α-phase of $CsPbI_3$ Perovskite by Sulfobetaine Zwitterions in One-Step Spin-Coating Films. *Joule* **2017,** 1, 371-382.

40. Swarnkar, A.; Marshall, A. R.; Sanehira, E. M.; Chernomordik, B. D.; Moore, D. T.; Christians, J. A.; Chakrabarti, T.; Luther, J. M., Quantum Dot–Induced Phase Stabilization of α-$CsPbI_3$ Perovskite for High-Efficiency Photovoltaics. *Science* **2016,** 354, 92-95.

41. Hamaguchi, R.; Yoshizawa-Fujita, M.; Miyasaka, T.; Kunugita, H.; Ema, K.; Takeoka, Y.; Rikukawa, M., Formamidine and cesium-based quasi-two-dimensional perovskites as photovoltaic absorbers. *Chem. Commun.* **2017,** 53, 4366-4369.

42. Liao, J.-F.; Rao, H.-S.; Chen, B.-X.; Kuang, D.-B.; Su, C.-Y., Dimension engineering on cesium lead iodide for efficient and stable perovskite solar cells. *J. Mater. Chem. A* **2017,** 5, 2066-2072.

43. Chang, J.; Zhang, S.; Wang, N.; Sun, Y.; Wei, Y.; Li, R.; Yi, C.; Wang, J.; Huang, W., Enhanced Performance of Red Perovskite Light-Emitting Diodes through the Dimensional Tailoring of Perovskite Multiple Quantum Wells. *J. Phys. Chem. Lett.* **2018,** 9, 881-886.f

44. Shpatz Dayan, A.; Cohen, B.-E.; Aharon, S.; Tenailleau, C.; Wierzbowska, M.; Etgar, L., Enhancing stability and photostability of $CsPbI_3$ by reducing its dimensionality. *Chem. Mater.* **2018,** 30, 8017-8024.

45. Mott, N. F.; Davis, E. A., *Electronic processes in non-crystalline materials*. OUP Oxford: 2012.

46. Shao, Y.; Yuan, Y.; Huang, J., Correlation of energy disorder and open-circuit voltage in hybrid perovskite solar cells. *Nature Energy* **2016,** 1, 15001.

47. Blakesley, J. C.; Neher, D., Relationship between energetic disorder and open-circuit voltage in bulk heterojunction organic solar cells. *Phys. Rev. B* **2011,** 84, 075210.

48. Heumueller, T.; Burke, T. M.; Mateker, W. R.; Sachs-Quintana, I. T.; Vandewal, K.; Brabec, C. J.; McGehee, M. D., Disorder-Induced Open-Circuit Voltage Losses in Organic Solar Cells During Photoinduced Burn-In. *Adv. Energy Mater.* **2015,** 5, 1500111.

49. Tai, Q.; You, P.; Sang, H.; Liu, Z.; Hu, C.; Chan, H. L. W.; Yan, F., Efficient and stable perovskite solar cells prepared in ambient air irrespective of the humidity. *Nat. Commun.* **2016,** 7, 11105.

50. Blancon, J. C.; Tsai, H.; Nie, W.; Stoumpos, C. C.; Pedesseau, L.; Katan, C.; Kepenekian, M.; Soe, C. M. M.; Appavoo, K.; Sfeir, M. Y., Extremely efficient internal exciton dissociation through edge states in layered 2D perovskites. *Science* **2017**, 355, 1288-1292.

51. Wang, K.; Wu, C.; Yang, D.; Jiang, Y.; Priya, S., Quasi-Two-Dimensional Halide Perovskite Single Crystal Photodetector. *ACS nano* **2018,** 12, 4919-4929.

52. Yan, K.; Long, M.; Zhang, T.; Wei, Z.; Chen, H.; Yang, S.; Xu, J., Hybrid halide perovskite solar cell precursors: colloidal chemistry and coordination engineering behind device processing for high efficiency. *J. Am. Chem. Soc.* **2015,** 137, 4460-4468.

53. Pérez-Gutiérrez, E.; Percino, M. J.; Montoya, D. M.; Solis-Ibarra, D.; Cerón, M.; Barbosa-García, O., Control of the Morphology and Crystallinity of a PbI_2 Layer for Large-Area Perovskite Films Prepared by Close Space Sublimation. *ACS Appl. Energy Mater.* **2018,** 1, 3843-3849.

54. Hu, Y.; Spies, L. M.; Alonso-Álvarez, D.; Mocherla, P.; Jones, H.; Hanisch, J.; Bein, T.; Barnes, P. R. F.; Docampo, P., Identifying and controlling phase purity in 2D hybrid perovskite thin films. *J. Mater. Chem. A* **2018,** 6, 22215-22225.

55. Cohen, B.-E.; Etgar, L., Parameters that control and influence the organo-metal halide perovskite crystallization and morphology. *Front. of Optoelectron.* **2016,** 9, 44-52.

56. Lee, J.-W.; Kim, H.-S.; Park, N.-G., Lewis acid–base adduct approach for high efficiency perovskite solar cells. *Acc. Chem. Res.* **2016,** 49, 311-319.

57. Gutmann, V.; Wychera, E., Coordination reactions in non aqueous solutions-The role of the donor strength. *Inorg. Nucl. Chem. Lett.* **1966,** 2, 257-260.

58. Hamill Jr, J. C.; Schwartz, J.; Loo, Y.-L., Influence of Solvent Coordination on Hybrid Organic–Inorganic Perovskite Formation. *ACS Energy Lett.* **2017,** 3, 92-97.

59. Foley, B. J.; Girard, J.; Sorenson, B. A.; Chen, A. Z.; Niezgoda, J. S.; Alpert, M. R.; Harper, A. F.; Smilgies, D.-M.; Clancy, P.; Saidi, W. A., Controlling nucleation, growth, and orientation of metal halide perovskite thin films with rationally selected additives. *J. Mater. Chem. A* **2017,** 5, 113-123.

60. Herbol, H. C.; Hu, W.; Frazier, P.; Clancy, P.; Poloczek, M., Efficient search of compositional space for hybrid organic–inorganic perovskites via Bayesian optimization. *NPJ Comput. Mater.* **2018,** 4, 51.

61. Reichardt, C.; Welton, T., *Solvents and solvent effects in organic chemistry*. John Wiley & Sons: 2011.

62. Lv, M.; Dong, X.; Fang, X.; Lin, B.; Zhang, S.; Ding, J.; Yuan, N., A promising alternative solvent of perovskite to induce rapid crystallization for high-efficiency photovoltaic devices. *RSC Adv.* **2015,** 5, 20521-20529.

63. Fang, X.; Wu, Y.; Lu, Y.; Sun, Y.; Zhang, S.; Zhang, J.; Zhang, W.; Yuan, N.; Ding, J., Annealing-free perovskite films based on solvent engineering for efficient solar cells. *J. Mater. Chem. C* **2017,** 5, 842-847.

64. Bao, X.; Wang, Y.; Zhu, Q.; Wang, N.; Zhu, D.; Wang, J.; Yang, A.; Yang, R., Efficient planar perovskite solar cells with large fill factor and excellent stability. *J. Power Sources* **2015,** 297, 53-58.

65. Wu, T.; Wu, J.; Tu, Y.; He, X.; Lan, Z.; Huang, M.; Lin, J., Solvent engineering for high-quality perovskite solar cell with an efficiency approaching 20%. *J. Power Sources* **2017,** 365, 1-6.

66. Jeon, Y.-J.; Lee, S.; Kang, R.; Kim, J.-E.; Yeo, J.-S.; Lee, S.-H.; Kim, S.-S.; Yun, J.-M.; Kim, D.-Y., Planar heterojunction perovskite solar cells with superior reproducibility. *Sci. Rep.* **2014,** 4, 6953.

67. Liang, K.; Mitzi, D. B.; Prikas, M. T., Synthesis and characterization of organic− inorganic perovskite thin films prepared using a versatile two-step dipping technique. *Chem. Mater.* **1998,** 10, 403-411.

68. Trots, D. M.; Myagkota, S. V., High-temperature structural evolution of caesium and rubidium triiodoplumbates. *J. Phys. Chem. Solids* **2008,** 69, 2520-2526.

69. Shahiduzzaman, M.; Yonezawa, K.; Yamamoto, K.; Ripolles, T. S.; Karakawa, M.; Kuwabara, T.; Takahashi, K.; Hayase, S.; Taima, T., Improved Reproducibility and Intercalation Control of Efficient Planar Inorganic Perovskite Solar Cells by Simple Alternate Vacuum Deposition of PbI_2 and CsI. *ACS Omega* **2017,** 2, 4464-4469.

70. Liu, M.; Voznyy, O.; Sabatini, R.; de Arquer, F. P. G.; Munir, R.; Balawi, A. H.; Lan, X.; Fan, F.; Walters, G.; Kirmani, A. R., Hybrid organic–inorganic inks flatten the energy landscape in colloidal quantum dot solids. *Nat. Mater.* **2017,** 16, 258.

71. Liu, Y.; Gibbs, M.; Puthussery, J.; Gaik, S.; Ihly, R.; Hillhouse, H. W.; Law, M., Dependence of carrier mobility on nanocrystal size and ligand length in PbSe nanocrystal solids. *Nano Lett.* **2010,** 10, 1960-1969.